


Strong ferromagnetic fluctuations in a doped checkerboard latticeYue Pan,¹ Runyu Ma^{1,2}  and Tianxing Ma^{1,3,*}¹*Department of Physics, Beijing Normal University, Beijing 100875, China*²*Beijing Computational Science Research Center, Beijing 100193, China*³*Key Laboratory of Multiscale Spin Physics (Ministry of Education), Beijing Normal University, Beijing 100875, China*

(Received 28 March 2023; revised 6 June 2023; accepted 6 June 2023; published 16 June 2023)

Using the determinant quantum Monte Carlo method, we study the magnetic susceptibility in the parameter space of the on-site interaction U , temperature T , electron filling $\langle n \rangle$, and the frustration control parameter t' within the Hubbard model on a two-dimensional checkerboard lattice. It is shown that the system exhibits stable and strong ferromagnetic fluctuations about the electron filling $\langle n \rangle \geq 1.2$ for different t' , and the ferromagnetic susceptibility is strongly enhanced by the increasing interaction and decreasing temperature. We also discuss the sign problem to clarify which parameter region is accessible and reliable. Our findings not only demonstrate important implications for modulating magnetism in the checkerboard lattice, but will also provide a theoretical platform for a flat-band model that demonstrates a variety of physical properties.

DOI: [10.1103/PhysRevB.107.245126](https://doi.org/10.1103/PhysRevB.107.245126)**I. INTRODUCTION**

Because of the discovery of doped graphene-based materials [1] and metal-doped transition-metal dichalcogenides (TMDs) [2], which have the capacity to control magnetic order through charge transfer, the possibility of manufacturing new magnetic devices has attracted much attention. Researchers are interested in semiconducting two-dimensional (2D) materials doped with impurity atoms, which are considered as a promising platform for high-performance spintronic devices and sensors. Magnetism plays an important role in the properties of these materials [3] and, in the past few years, people have had great interest in the properties of quantum magnets with geometric frustration [4], such as organic charge transfer salts of triangular lattices [5], compounds of kagome lattices [6–9], and so on, which are expected to describe novel quantum states and interesting magnetic phases in this field, including quantum spin liquid [10], and spin ice [11–13]. Additionally, pyrochlore oxides such as LiV_2O_4 [14,15] and $\text{Sn}_2\text{X}_2\text{O}_7$ ($X = \text{Nb}, \text{Ta}$) [16,17] represent another geometric frustration structure, i.e., the checkerboard lattice [18], which attracts intensive studies due to its rich phase diagram induced by electronic correlation, including the quantum Hall effect [19], superconductivity [20], Mott physics [21,22], and other phenomena. One promising candidate is $\text{Sn}_2\text{X}_2\text{O}_7$ ($X = \text{Nb}, \text{Ta}$), which shows possible ferromagnetism induced by the quasi-flat band [17].

Most of the previous theoretical investigations primarily focused on the checkerboard lattice at half filling. Based on the Heisenberg model with spin exchange coupling interaction [23,24], rich magnetic characteristics such as valence-bond crystal phases [25], and various magnetization plateaus [26] have been proposed. The ground-state properties of the

geometrically frustrated Hubbard model on the anisotropic checkerboard lattice at half filling have been studied using the path-integral renormalization group method [27–29]. It was found that the increase of the Coulomb interaction may induce the first-order metal-insulator transition to the antiferromagnetically ordered phase [27], and the plaquette-singlet insulator may emerge besides the antiferromagnetic insulator and the paramagnetic metal, depending on the frustration-control parameter [29]. However, intriguing physical phenomena always arise as the system is doped. For a simple square lattice, it is well known that it is a Mott insulator with antiferromagnetic Néel order for all values of $U > 0$ [30–33]. By using various approaches, including determinant quantum Monte Carlo (DQMC) [34–36], variational Monte Carlo (VMC) [37,38], and dynamic cluster approximation (DCA) [39], there is evidence that the doped square lattice exhibits many of the basic physical properties which characterize the unconventional superconductors [40,41], for example, antiferromagnetic spin fluctuations [42,43], pseudogap [44–46], and nematic correlations [47], as well as stripes [48]. Besides these, a doping-dependent metal-insulator transition in the disordered Hubbard model on a square lattice [49,50] and the possible controllability of ferromagnetism in a doped honeycomb lattice [51] are also proposed. These stimulate us to investigate the properties of a checkerboard lattice at finite doping, especially the evolution of magnetic characteristics. Since the checkerboard lattice contains frustration and a flat band, which the square lattice does not possess, it would be an interesting topic to study how strong ferromagnetic fluctuations emerge in a doped Hubbard model on a checkerboard lattice.

In the checkerboard lattice, there are two nonequivalent sites per unit cell of the square lattice, defining two interpenetrating sublattices, as illustrated in Fig. 1(a), where t represents the nearest hopping and t' indicating the next-nearest hopping. Figure 1(b) shows the high-symmetry lines

*txma@bnu.edu.cn

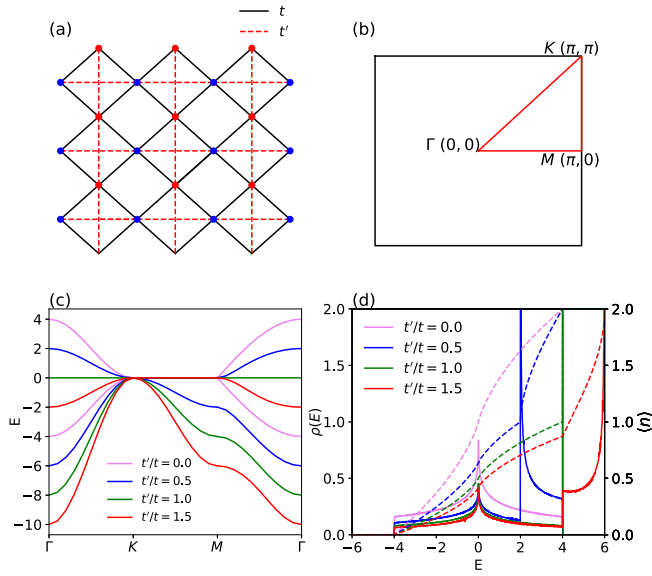


FIG. 1. (a) Sketch of checkerboard lattice. (b) The first Brillouin zone and the high-symmetry direction (red line). (c) The energy band along the high-symmetry direction. (d) DOS (solid lines) and filling n (dashed lines) as functions of energy.

of the first Brillouin zone. In Fig. 1(c), one can see that the checkerboard lattice exhibits an energetically flat band that is in touch with a quadratically dispersive band along with high-symmetry lines of the first Brillouin zone in k space. The density of states (DOS) is shown in Fig. 1(d), and there is van Hove singularity in its shape at different fillings that depend on the value of t' . Usually, the interplay between electronic correlation and flat band, or van Hove singularity, may lead to strong ferromagnetic fluctuations. The magnetic exchange between local spins is largely dominated by the contribution of the flat band, which is ferromagnetic, as revealed by many studies [52–56].

In this work, we will further provide an intensive numerical simulation on the magnetism of the doped Hubbard model on a checkerboard lattice using the DQMC method. The checkerboard lattice that we construct can be realized and modulated through considering next-nearest-neighbor hopping t' as the frustration-control parameter, to study the effect of the geometric frustration and doping on the magnetic order at finite temperatures and to interpret the observed magnetic behavior as a result of electronic correlation and the synergetic effect of a special lattice geometry. We also discuss the sign problem to determine which parameter regions are accessible and unreliable. Interestingly, we found that the system showed obvious ferromagnetism when the electron filling is $n \geq 1.2$, and it is stable and strongest at approximately $n \approx 1.5$. The strong ferromagnetic fluctuations we revealed can be understood in the framework of the flat-band scenario.

II. MODEL AND METHODS

We consider the Hubbard model defined on a two-dimensional checkerboard lattice. The checkerboard lattice possesses two sublattices, so the number of total lattice sites

is $2 \times L^2$. The Hamiltonian that we studied is given by

$$\begin{aligned} \mathcal{H} &= \mathcal{H}_1 + \mathcal{H}_2 + \mathcal{H}_3 + \mathcal{H}_4, \\ \mathcal{H}_1 &= -t \sum_{(i,j)\sigma} (c_{iA\sigma}^\dagger c_{jB\sigma} + \text{H.c.}), \\ \mathcal{H}_2 &= -t' \sum_{i\sigma} (c_{iA\sigma}^\dagger c_{i+xA\sigma} + c_{iA\sigma}^\dagger c_{i-xA\sigma} + \text{H.c.}), \\ \mathcal{H}_3 &= -t' \sum_{j\sigma} (c_{iB\sigma}^\dagger c_{i+yB\sigma} + c_{iB\sigma}^\dagger c_{i-yB\sigma} + \text{H.c.}), \\ \mathcal{H}_4 &= U \sum_{il} n_{il\uparrow} n_{il\downarrow} + \mu \sum_{il\sigma} n_{il\sigma}, \end{aligned} \quad (1)$$

where t is the hopping amplitude between the nearest-neighbor sites on the lattice. We set $t = 1$ as a unit of energy, where t' is the next-nearest-neighbor (NNN) hopping integral and $c_{il\sigma}^\dagger$ ($c_{il\sigma}$) indicates the creation (annihilation) of an electron at a site i . The sublattice is l and the spin is σ . $n_{il\sigma} = c_{il\sigma}^\dagger c_{il\sigma}$ is the corresponding particle number operator and $\langle i, j \rangle$ denotes the nearest neighbor. The second term \mathcal{H}_2 represents the next-nearest hopping term of the A sublattice, where only the hoppings in the x direction are considered. The third term \mathcal{H}_3 represents the next nearest B sublattice, and only the y -direction hoppings are considered. The last term contains the Hubbard interaction U , which is the strength of the electron repulsion, and the chemical potential μ , which tunes the electron filling.

We can carry out a Fourier transformation $c_{kl\sigma} = \sum_j e^{ijR} c_{jl\sigma}$ to extract the band structure in the noninteracting limit ($U \rightarrow 0$). After Fourier transformation, the noninteracting Hamiltonian can be block diagonalized to $\mathcal{H} = \sum_k \mathcal{H}(k)$, and $\mathcal{H}(k)$ can be written as

$$H = \sum_{\mathbf{k}\sigma} \begin{pmatrix} c_{\mathbf{k}1\sigma}^\dagger & c_{\mathbf{k}2\sigma}^\dagger \end{pmatrix} \begin{pmatrix} \alpha_{\mathbf{k}} & \beta_{\mathbf{k}} \\ \beta_{\mathbf{k}} & \gamma_{\mathbf{k}} \end{pmatrix} \begin{pmatrix} c_{\mathbf{k}1\sigma} \\ c_{\mathbf{k}2\sigma} \end{pmatrix}, \quad (2)$$

where

$$\begin{aligned} \beta_{\mathbf{k}} &= -2t \left[\cos \frac{\mathbf{k}}{2} \cdot (\vec{a}_1 + \vec{a}_2) + \cos \frac{\mathbf{k}}{2} \cdot (\vec{a}_1 - \vec{a}_2) \right], \\ \alpha_{\mathbf{k}} &= -2t' \cos \mathbf{k} \cdot \vec{a}_1, \\ \gamma_{\mathbf{k}} &= -2t' \cos \mathbf{k} \cdot \vec{a}_2. \end{aligned} \quad (3)$$

The unit vector $\vec{a}_1 = (1, 0)$, $\vec{a}_2 = (0, 1)$. Diagonalizing this matrix can transform the Hamiltonian into a band basis, and the two eigenvalues of this matrix are $E^\pm(k) = 1/2[\alpha_{\mathbf{k}} + \beta_{\mathbf{k}}] \pm 1/2\sqrt{\alpha_{\mathbf{k}}^2 - 2\alpha_{\mathbf{k}}\gamma_{\mathbf{k}} + 4\beta_{\mathbf{k}}^2 + \gamma_{\mathbf{k}}^2}$. The band structure is plotted in Fig. 1(c), where we can see that the flat band starts to develop when the t' term is introduced, and the upper band becomes completely flat when $t'/t = 1$.

We perform DQMC [57–59] simulations to extract the finite-temperature properties of a checkerboard lattice at different fillings and different t'/t values. The main principle of the DQMC algorithm is as follows: first, the partition function $\mathcal{Z} = \text{Tr} e^{-\beta\mathcal{H}}$ is expressed in a discretized imaginary-time slice, and this step is called the Trotter decomposition. Next, we decouple the interaction term by the Hubbard-Stratonovich (HS) transformation [34,59]. After this step, an auxiliary field couples to electrons and the interaction term disappears. Then,

we can trace out the electron freedom and the resulting determinant becomes the weight in the sampling process. The observable can be written as $\langle O \rangle = \frac{\text{Tr}[e^{-\beta H} O]}{\mathcal{Z}} = \sum_s \mathbf{P}_s \langle O \rangle_s$, where the weight is $\mathbf{P}_s = \frac{\det[1+B_s(\beta,0)]}{\sum_s \det[1+B_s(\beta,0)]}$ and, in practice, the sampling used is based on a single-flip algorithm, and the accept ratio is $R = \frac{\mathbf{P}_{s'}}{\mathbf{P}_s}$. Green functions of certain auxiliary field configurations can be computed by the formula $G^\sigma = [I + \prod_l B_l^\sigma]^{-1}$. The B matrix introduced above is $B_l^\sigma = e^{\sigma \Delta \tau \lambda_s} e^{-\Delta \tau H_0}$, and s_l is the auxiliary field introduced, λ is the corresponding coefficient, and H_0 is the noninteracting part of the Hamiltonian. One should note that after HS transformation, the action becomes bilinear and the correlations can be calculated by using the Wick theorem; then, all observables can be calculated by Green functions. In practice, we start at a random initialized auxiliary field; then we conduct a warm-up process without calculating observables. Next, we conduct several measurements to accumulate observables into bins. In our simulations, we use 8000 sweeps to equilibrate the system and an additional $\sim 10\,000$ – $200\,000$ sweeps to generate measurements, which were split into 10 bins to provide the basis of the coarse-grain averages. The validity of this method has been verified in many previous studies, including doped graphene [51], an iron-based superconductor [60], as well as a highly geometry-frustrated system [61].

To study ferromagnetic fluctuations, we define the spin susceptibility in the z direction at zero frequency,

$$\chi(q) = \frac{1}{N} \sum_{i,j} \sum_{l,m} \int_0^\beta d\tau e^{-iq(\mathbf{R}_i - \mathbf{R}_j)} \langle S_{i,l}^z(\tau) S_{j,m}^z(0) \rangle, \quad (4)$$

where $S_{i,l}^z(\tau) = e^{H\tau} S_{j,m}^z(0) e^{-H\tau}$ with $S_{i,l}^z = c_{i,l}^\dagger c_{i,l} - c_{i,l}^\dagger c_{i,l}$. To have a deep understanding of the effect of t'/t on the magnetic order, we look at the spin susceptibility as a function of temperature T , interaction U , and electronic filling n on a $L = 8$ lattice for several typical $t'/t = 0.25 \sim 1.50$.

III. RESULTS AND DISCUSSION

In Fig. 2, we show the magnetic susceptibility $\chi(q)$ along with high-symmetry lines of the first Brillouin zone including $\Gamma = (0, 0)$, $K = (\pi, \pi)$, and $M = (\pi, 0)$. We can see that the t'/t term has a significant effect at $U = 3.0t$, $T = t/6$, with different filling (a) $n = 1.30$, (b) $n = 1.40$, (c) $n = 1.50$, and (d) $n = 1.60$. $\chi(\Gamma)$ gets enhanced greatly as t'/t increases, while $\chi(K)$ increases only slightly. The change of $\chi(\Gamma)$ is considered to be a significant ferromagnetic fluctuation with increasing t'/t . And we may also notice that $\chi(\Gamma)$ have a peak at $t' = 1$, where the upper band is a flat band. This reflects the importance of the flat band and electron structure in the shaping of ferromagnetic behavior. To understand the filling dependence of magnetic correlations in a checkerboard lattice, we show, in Fig. 3, the magnetic susceptibilities for ferromagnetic fluctuation $\chi(\Gamma)$ and antiferromagnetic fluctuation $\chi(K)$ at $T = t/6$ and $U = 3.0t$ with different values of t'/t , (a) $t'/t = 0.50$, (b) $t'/t = 0.75$, (c) $t'/t = 1.00$, and (d) $t'/t = 1.25$. Here we can see that $\chi(\Gamma)$ increases faster than $\chi(K)$ at filling in the range 1.20 to 1.60, and $\chi(\Gamma)$ becomes higher than $\chi(K)$, indicating that ferromagnetic fluctuation is dominant. We also see the maximum of magnetic

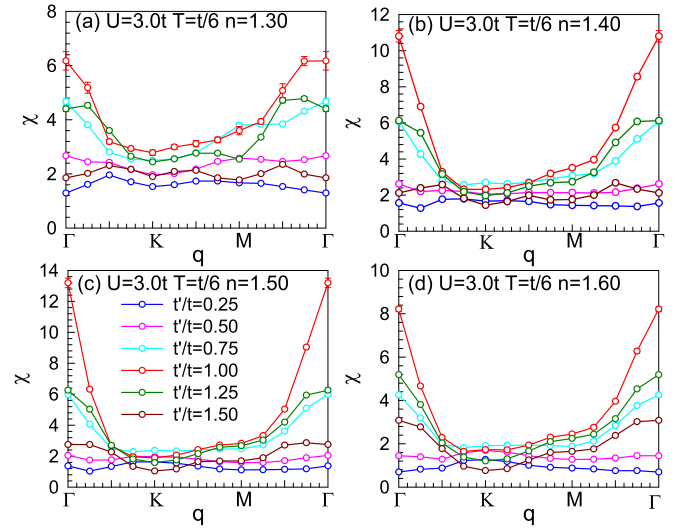


FIG. 2. Magnetic susceptibility vs momentum q at different t'/t . Here, $U = 3.0t$, $T = t/6$ for (a) $n = 1.30$, (b) $n = 1.40$, (c) $n = 1.50$, and (d) $n = 1.60$.

susceptibilities at approximately $n \approx 1.5$, which is stable and the strongest ferromagnetic fluctuation.

Then, we investigate the properties of ferromagnetic correlation at a fixed electron filling $n = 1.50$. In Figs. 4(a) and 4(b), we show the magnetic susceptibility at the filling $n = 1.50$, $U = 3.0t$, $t'/t = 0.75$, and $t'/t = 1.00$. For temperature T ranging from $1/2$ to $1/8$, the magnetic susceptibility increases as T decreases. In Figs. 4(c) and 4(d), we show the magnetic susceptibility at the filling $n = 1.50$, $t'/t = 0.75$, and $t'/t = 1.00$. For U ranging from 1.0 to 4.0 and temperature $T = t/6$, the magnetic susceptibility increases as U increases. This reflects the enhancement of ferromagnetic correlation by interaction U .

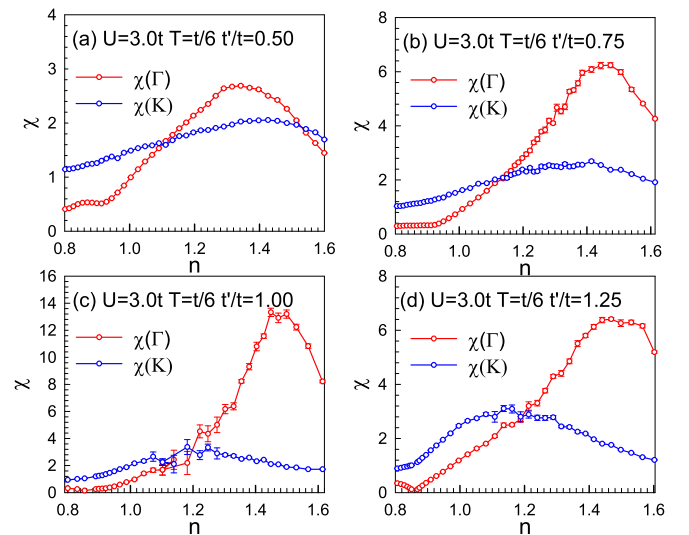


FIG. 3. Magnetic susceptibility $\chi(\Gamma)$ (red) and $\chi(K)$ (blue) vs electron filling n at $U = 3.0t$, $T = t/6$ with (a) $t'/t = 0.50$, (b) $t'/t = 0.75$, (c) $t'/t = 1.00$, and (d) $t'/t = 1.25$.

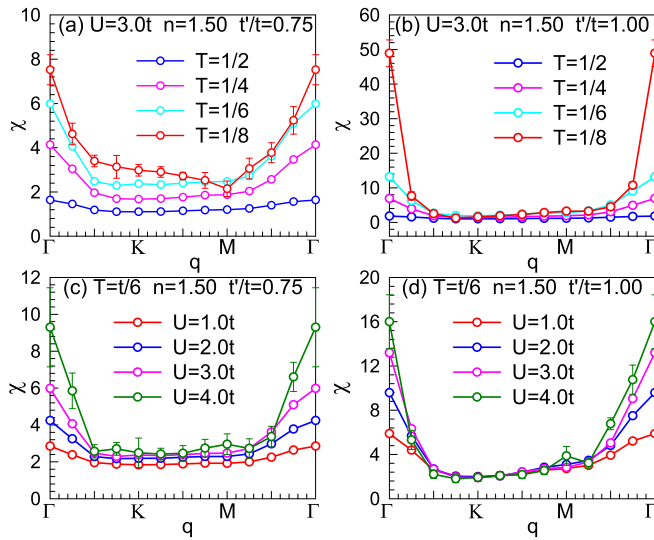


FIG. 4. The magnetic susceptibility vs the momentum q at different values of T with $U = 3.0t$, $n = 1.50$, (a) $t'/t = 0.75$, and (b) $t'/t = 1.00$. The magnetic susceptibility vs the momentum q at different values of U with $T = t/6$, $n = 1.50$, (c) $t'/t = 0.75$, and (d) $t'/t = 1.00$.

Then, we present the temperature dependence of the magnetic susceptibility at $n = 1.50$ with different U and t'/t in Figs. 5(a) and 5(b). The figure exhibits a linear correlation between $1/\chi$ and temperature T , which corresponds to the Curie-Weiss behavior $1/\chi = (T - T_c)/A$. Therefore, we extrapolate $1/\chi$ to zero temperature by using linear fitting. If the system possesses a finite T_c , its intercept should be negative. Figure 5(a) shows that the on-site interaction U enhances the ferromagnetic fluctuations and the negative intercept appears at approximately $U = 2.0t$. Figure 5(b) shows that the fully frustrated case $t'/t = 1.0$ has the lowest intercept, which means it has the highest T_c .

According to previous studies, the sign problem is a major obstacle to reaching low temperatures and strong-coupling regions in the QMC simulations. In Fig. 6, the average sign evolves with electron filling n , while other parameters are fixed, for a doped checkerboard lattice. In our simulations, especially in the following simulation results where the sign problem is much worse, we have increased the measurement

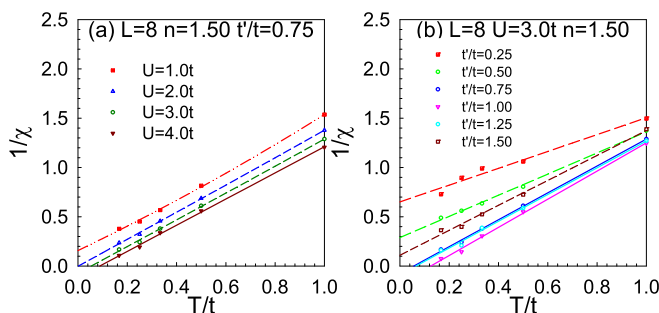


FIG. 5. (a) The temperature-dependent $1/\chi$ at $n = 1.50$ and $t'/t = 0.75$ with different U . (b) The temperature-dependent $1/\chi$ at $U = 3.0t$ and $n = 1.50$ with different t'/t .

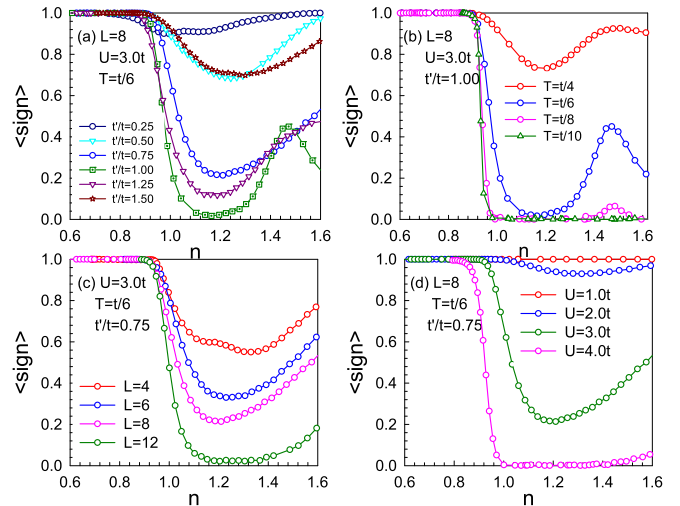


FIG. 6. The average sign as a function of electron filling n for (a) different t'/t , (b) different temperature T , (c) different lattice sizes L , and (d) different interactions U .

from $\sim 10\,000$ – $200\,000$ times to compensate for the fluctuations, which is large enough to ensure the reliability and accuracy of the data [62]. Figure 6 plots the average sign with different values of t'/t [Fig. 6(a)], different temperatures T [Fig. 6(b)], different lattice sizes L [Fig. 6(c)], and different interactions U [Fig. 6(d)].

In Fig. 6(a), the sign problem becomes worse along with hopping strength t' , which increases at first and then decreases as the value of t'/t continuously increases. Particularly, when $t'/t = 1.00$, it is shown that the average sign falls to a minimum value. We note another universal feature for all values of t' , which is that $\langle \text{sign} \rangle$ presents a minimum at the electron filling n around 1.20. As shown in the analysis of magnetism in Fig. 3, we find that the value where ferromagnetic fluctuations become dominant is also $n \approx 1.20$. It has been reported that $\langle \text{sign} \rangle$ can be related to the quantum phase transition [63]. So, this minimum in the $\langle \text{sign} \rangle$ may come out of the ferromagnetism.

In Fig. 6(b), the average sign decays exponentially with decreasing temperature. The average sign is almost zero when $n > 1.00$ at the temperatures $T = t/8$ and $T = t/10$, making the DQMC simulations nearly impossible. Moreover, by comparing various values of lattice size L for the $t'/t = 0.75$, we know that as the lattice size increases, the value of the average sign decreases, as shown in Fig. 6(c). In Fig. 6(d), for values of U in the range 1.0 to 4.0 with the temperature fixed at $T = t/6$, the sign problem becomes worse as U becomes larger.

IV. CONCLUSIONS

In this work, we study the finite-temperature properties of the checkerboard lattice Hubbard model by means of the DQMC method. Our results present exact numerical results on the magnetic correlation. By controlling the geometric frustration via a systematic change in the transfer integral t' along the diagonal bonds, we show the wide parameter region from $t'/t = 0.25$ to $t'/t = 1.50$, including the fully frustrated checkerboard lattice $t'/t = 1.00$, where there is a

stable ferromagnetic state at electron filling $n = 1.5$ for a certain temperature, and this effect is obviously strengthened as the interaction U increases. We also discuss the sign problem to clarify which parameter regions are accessible and reliable. Our findings not only have important implications for exploiting emergent flat-band physics in special lattice geometries, but also may shed light on the competition between the magnetic modes of highly frustrated systems. Therefore,

we provide further guidance for experiments in this parameter space.

ACKNOWLEDGMENTS

This work was supported by NSFC (Grant No. 11974049). The numerical simulations in this work were performed at HSCC of Beijing Normal University.

-
- [1] J. Červenka, M. Katsnelson, and C. Flipse, *Nat. Phys.* **5**, 840 (2009).
- [2] P. D. Reyntjens, S. Tiwari, M. L. V. de Put, B. Sorée, and W. G. Vandenberghe, *2D Mater.* **8**, 025009 (2021).
- [3] B. Fauqué, Y. Sidis, V. Hinkov, S. Pailhès, C. T. Lin, X. Chaud, and P. Bourges, *Phys. Rev. Lett.* **96**, 197001 (2006).
- [4] A. Ramirez, *Nature (London)* **421**, 483 (2003).
- [5] P. Lunkenheimer, J. Müller, S. Krohns, F. Schrettle, A. Loidl, B. Hartmann, R. Rommel, M. De Souza, C. Hotta, J. A. Schlueter *et al.*, *Nat. Mater.* **11**, 755 (2012).
- [6] Z. Lin, J.-H. Choi, Q. Zhang, W. Qin, S. Yi, P. Wang, L. Li, Y. Wang, H. Zhang, Z. Sun, L. Wei, S. Zhang, T. Guo, Q. Lu, J.-H. Cho, C. Zeng, and Z. Zhang, *Phys. Rev. Lett.* **121**, 096401 (2018).
- [7] H. Li, T. T. Zhang, T. Yilmaz, Y. Y. Pai, C. E. Marvinney, A. Said, Q. W. Yin, C. S. Gong, Z. J. Tu, E. Vescovo, C. S. Nelson, R. G. Moore, S. Murakami, H. C. Lei, H. N. Lee, B. J. Lawrie, and H. Miao, *Phys. Rev. X* **11**, 031050 (2021).
- [8] X. Wu, T. Schwemmer, T. Müller, A. Consiglio, G. Sangiovanni, D. Di Sante, Y. Iqbal, W. Hanke, A. P. Schnyder, M. M. Denner, M. H. Fischer, T. Neupert, and R. Thomale, *Phys. Rev. Lett.* **127**, 177001 (2021).
- [9] M. M. Denner, R. Thomale, and T. Neupert, *Phys. Rev. Lett.* **127**, 217601 (2021).
- [10] T. Eschmann, P. A. Mishchenko, T. A. Bojesen, Y. Kato, M. Hermanns, Y. Motome, and S. Trebst, *Phys. Rev. Res.* **1**, 032011(R) (2019).
- [11] L. Balents, *Nature (London)* **464**, 199 (2010).
- [12] S. Fujimoto, *Phys. Rev. B* **67**, 235102 (2003).
- [13] S. Fujimoto, *Phys. Rev. Lett.* **89**, 226402 (2002).
- [14] K. Tomiyasu, K. Iwasa, H. Ueda, S. Niitaka, H. Takagi, S. Ohira-Kawamura, T. Kikuchi, Y. Inamura, K. Nakajima, and K. Yamada, *Phys. Rev. Lett.* **113**, 236402 (2014).
- [15] T. Yajima, T. Soma, K. Yoshimatsu, N. Kurita, M. Watanabe, and A. Ohtomo, *Phys. Rev. B* **104**, 245104 (2021).
- [16] N. Kikuchi, A. Samizo, S. Ikeda, Y. Aiura, K. Mibu, and K. Nishio, *Phys. Rev. Mater.* **1**, 021601(R) (2017).
- [17] I. Hase, T. Yanagisawa, Y. Aiura, and K. Kawashima, *Phys. Rev. Lett.* **120**, 196401 (2018).
- [18] B. Javanparast, Z. Hao, M. Enjalran, and M. J. P. Gingras, *Phys. Rev. Lett.* **114**, 130601 (2015).
- [19] W. Li, D. N. Sheng, C. S. Ting, and Y. Chen, *Phys. Rev. B* **90**, 081102(R) (2014).
- [20] E. Santos, J. Iglesias, C. Lacroix, and M. Gusmão, *J. Phys.: Condens. Matter* **22**, 215701 (2010).
- [21] N. Swain, R. Tiwari, and P. Majumdar, *Phys. Rev. B* **94**, 155119 (2016).
- [22] S. Fujimoto, *Phys. Rev. B* **64**, 085102 (2001).
- [23] S. Capponi, *Phys. Rev. B* **95**, 014420 (2017).
- [24] Y. Xu, Z. Xiong, H.-Q. Wu, and D.-X. Yao, *Phys. Rev. B* **99**, 085112 (2019).
- [25] E. Khatami and M. Rigol, *Phys. Rev. B* **83**, 134431 (2011).
- [26] K. Morita and N. Shibata, *Phys. Rev. B* **94**, 140404(R) (2016).
- [27] T. Yoshioka, A. Koga, and N. Kawakami, *J. Magn. Magn. Mater.* **310**, 873 (2007).
- [28] T. Yoshioka, A. Koga, and N. Kawakami, *J. Phys. Soc. Jpn.* **77**, 104702 (2008).
- [29] T. Yoshioka, A. Koga, and N. Kawakami, *Phys. Rev. B* **78**, 165113 (2008).
- [30] Y. Claveau, B. Arnaud, and S. D. Matteo, *Eur. J. Phys.* **35**, 035023 (2014).
- [31] S. V. Kravchenko, G. V. Kravchenko, J. E. Furneaux, V. M. Pudalov, and M. D'Iorio, *Phys. Rev. B* **50**, 8039 (1994).
- [32] S. V. Kravchenko, W. E. Mason, G. E. Bowker, J. E. Furneaux, V. M. Pudalov, and M. D'Iorio, *Phys. Rev. B* **51**, 7038 (1995).
- [33] S. V. Kravchenko, D. Simonian, M. P. Sarachik, W. Mason, and J. E. Furneaux, *Phys. Rev. Lett.* **77**, 4938 (1996).
- [34] S. R. White, D. J. Scalapino, R. L. Sugar, E. Y. Loh, J. E. Gubernatis, and R. T. Scalettar, *Phys. Rev. B* **40**, 506 (1989).
- [35] J. E. Hirsch, *Phys. Rev. B* **31**, 4403 (1985).
- [36] T. Paiva, R. T. Scalettar, C. Huscroft, and A. K. McMahan, *Phys. Rev. B* **63**, 125116 (2001).
- [37] C. Gros, *Phys. Rev. B* **38**, 931 (1988).
- [38] A. Paramekanti, M. Randeria, and N. Trivedi, *Phys. Rev. B* **70**, 054504 (2004).
- [39] M. Jarrell, T. Maier, C. Huscroft, and S. Moukouri, *Phys. Rev. B* **64**, 195130 (2001).
- [40] T. Hanaguri, C. Lupien, Y. Kohsaka, D.-H. Lee, M. Azuma, M. Takano, H. Takagi, and J. Davis, *Nature (London)* **430**, 1001 (2004).
- [41] M. Abdel-Hafiez, Y.-Y. Zhang, Z.-Y. Cao, C.-G. Duan, G. Karapetrov, V. M. Pudalov, V. A. Vlasenko, A. V. Sadakov, D. A. Knyazev, T. A. Romanova, D. A. Chareev, O. S. Volkova, A. N. Vasiliev, and X.-J. Chen, *Phys. Rev. B* **91**, 165109 (2015).
- [42] F. Šimkovic, J. P. F. LeBlanc, A. J. Kim, Y. Deng, N. V. Prokof'ev, B. V. Svistunov, and E. Kozik, *Phys. Rev. Lett.* **124**, 017003 (2020).
- [43] A. Wietek, Y.-Y. He, S. R. White, A. Georges, and E. M. Stoudenmire, *Phys. Rev. X* **11**, 031007 (2021).
- [44] C. Huscroft, M. Jarrell, T. Maier, S. Moukouri, and A. N. Tahvildarzadeh, *Phys. Rev. Lett.* **86**, 139 (2001).
- [45] B. D. Faeth, S.-L. Yang, J. K. Kawasaki, J. N. Nelson, P. Mishra, C. T. Parzyck, C. Li, D. G. Schlom, and K. M. Shen, *Phys. Rev. X* **11**, 021054 (2021).
- [46] B. Kyung, V. Hankevych, A.-M. Daré, and A. M. S. Tremblay, *Phys. Rev. Lett.* **93**, 147004 (2004).

- [47] S.-Q. Su and T. A. Maier, *Phys. Rev. B* **84**, 220506(R) (2011).
- [48] D. J. Scalapino, *Rev. Mod. Phys.* **84**, 1383 (2012).
- [49] P. J. H. Denteneer, R. T. Scalettar, and N. Trivedi, *Phys. Rev. Lett.* **83**, 4610 (1999).
- [50] L. Tian, Y. Li, Y. Liang, and T. Ma, *Phys. Rev. B* **105**, 045132 (2022).
- [51] T. Ma, F. Hu, Z. Huang, and H.-Q. Lin, *Appl. Phys. Lett.* **97**, 112504 (2010).
- [52] J. Huang, Z. Wang, H. Pang, H. Wu, H. Cao, S.-K. Mo, A. Rustagi, A. F. Kemper, M. Wang, M. Yi, and R. J. Birgeneau, *Phys. Rev. B* **103**, 165105 (2021).
- [53] F. F. Tafti, J. J. Ishikawa, A. McCollam, S. Nakatsuji, and S. R. Julian, *Phys. Rev. B* **85**, 205104 (2012).
- [54] R. Liu, W. Nie, and W. Zhang, *Sci. Bull.* **64**, 1490 (2019).
- [55] L. S. G. Leite and R. L. Doretto, *Phys. Rev. B* **104**, 155129 (2021).
- [56] L. S. G. Leite and R. L. Doretto, *Phys. Rev. B* **106**, 155142 (2022).
- [57] R. R. dos Santos, *Braz. J. Phys.* **33**, 36 (2003).
- [58] J. E. Hirsch, *Phys. Rev. B* **28**, 4059 (1983).
- [59] R. Blankenbecler, D. J. Scalapino, and R. L. Sugar, *Phys. Rev. D* **24**, 2278 (1981).
- [60] T. Ma, H.-Q. Lin, and J. Hu, *Phys. Rev. Lett.* **110**, 107002 (2013).
- [61] F. M. Hu, S. Q. Su, T. X. Ma, and H. Q. Lin, *Phys. Rev. B* **80**, 014428 (2009).
- [62] T. Huang, L. Zhang, and T. Ma, *Sci. Bull.* **64**, 310 (2019).
- [63] R. Mondaini, S. Tarat, and R. T. Scalettar, *Science* **375**, 418 (2022).